Draft version September 29, 2015
Preprint typeset using LaTeX style emulateapj v. 05/12/14

# "HOT" NON-FLARING PLASMA IN ACTIVE REGIONS II. IMPACTS OF TWO-FLUID EFFECTS

W. T. Barnes and S. J. Bradshaw
Department of Physics & Astronomy, Rice University, Houston, TX 77251-1892

P. J. Cargill
Space and Atmospheric Physics, The Blackett Laboratory, Imperial College, London SW7 2BW and
School of Mathematics and Statistics, University of St. Andrews, St. Andrews, Scotland KY16 9SS
*Draft version September 29, 2015*

## ABSTRACT

Faint, high-temperature emission in active region cores has long been predicted as a signature of nanoflare heating. However, the detection of such emission has proved difficult due to a combination of the efficiency of thermal conduction, non-equilibrium ionization, and inadequate instrument sensitivity. This second paper in our series on hot non-flaring plasma in active regions aims to show how the assumption of electron-ion equilibrium in hydrodynamic models leads to incorrect conclusions regarding the hot emission. We have used an efficient two-fluid hydrodynamic model to carry out a parameter exploration in preferentially heated species, nanoflare heating frequency, and event amplitude power-law index. By computing the emission measure distributions and calculating their "hotward" slopes, we have concluded that the assumption of electron-ion equilibrium leads to an underestimate of the amount of hot plasma at intermediate and high heating frequencies. Additionally, we find that, while emission due to electron and ion heating differs greatly hotward of the peak, the respective coolward emission measure slopes are similar such that a distinction between the heating of one species over another based on this criteria alone is inadequate.

## 1. INTRODUCTION

Need to reword this introduction; move from introduction of hot plasma as signature of nanoflares to observational evidence for nanoflares and why it is hard to come by; to models which show evidence of nanoflares; to what we will do in this paper

The nanoflare heating model, first proposed by Parker (1988), has become one of the most favored and contentious coronal heating models (Cargill 1994; Cargill & Klimchuk 2004; Klimchuk 2006). While many theoretical efforts (e.g. Bradshaw et al. 2012; Reep et al. 2013) have shown the feasability of nanoflares, the idea has long suffered from a lack observational evidence. The term *nanoflare* has now become synonomous with impulsive heating in the energy range $10^{24} - 10^{27}$ ergs, with no specific assumption as to what underlying physical mechanism is responsible. However, while we ascribe no particular source (e.g. wave versus reconnection) to this bursty energy release, its origin is almost certainly magnetic.

Cargill (1994); Cargill & Klimchuk (2004) have predicted that emission measure distributions resulting from nanoflare models should be wide and have a faint, high-temperature ($> 4 \times 10^6$ K) component and thus a steep hotward slope. Unfortunately, observing this high-temperature emission is difficult and in some cases impossible. The reason for this difficulty is twofold. First, thermal conduction is a very efficient cooling mechanism at high temperatures and large spatial temperature gradients. When a loop is heated impulsively, its temperature rises quickly while the increase in density lags behind. By the time the density has increased sufficiently to allow for an appreciable amount of emission (recalling EM $\propto n^2$), thermal conduction has cooled the loop far below its initial hot temperature, making a direct detection of $> 10$ MK plasma very difficult.

The second reason for this difficulty is non-equilibrium ionization. It is usually assumed that the observed line intensities, because of their known formation temperatures, are a direct indicator of the plasma temperature. However, if the heating timescale is shorter than the ionization timescale, the time it takes for the ion population to settle into the correct charge state, an equilibrium assumption can lead to a misdiagnosis of the plasma temperature. This makes signatures of hot, nanoflare-heated plasma especially difficult to detect if the high temperatures persist for less than the ionization timescale (Bradshaw & Cargill 2006; Bradshaw & Klimchuk 2011; Reale & Orlando 2008).

Despite these difficulties, various attempts have been made to observe this faint high-temperature emission. Using the broadband X-Ray Telescope (XRT) aboard the *Hinode* spacecraft, Schmelz et al. (2009) and Reale et al. (2009) show a faint hot component in the reconstructed DEM curves. However, since the channels on such broadband instruments can often be polluted by low-temperature emission, the reliability of such measurements depends on the filtering technique used. Additionally, Winebarger et al. (2012) showed that combinations of *Hinode*/EIS and *Hinode*/XRT measurements leave a "blind spot" in the EM $- T$ space conincident with where evidence for nanoflare heating is likely to be found.

Unambiguous observational evidence of nanoflare heating must come from pure spectroscopic measurements (see Brosius et al. 2014). Additionally, new instruments

will.t.barnes@rice.edu

with higher spatial and temporal resolution, such as *IRIS* (De Pontieu et al. 2014) and the *Hi-C* sounding rocket (Cirtain et al. 2013) have provided encouraging results for impulsive heating (Testa et al. 2013, 2014). Future missions like the Marshall Grazing Incidence X-ray Spectrometer (MaGIXS) (Kobayashi et al. 2011; Winebarger 2014), with a wavelength range of 6-24 Å and a temperature range of $6.2 < \log T < 7.2$, aim to probe this previously poorly-resolved portion of the coronal spectrum in hopes of better quantifying the presence of faint, high-temperature plasma.

Need paragraph here saying something about two-fluid approach: why is it important in nanoflare heating scenarios?

Wouldn't be a bad idea to include summary of measured "hotward" emission slope values as is done in Bradshaw et al. (2013) for cool slopes

In this paper, the second in our series on hot emission in active region cores, we will use an efficient two-fluid hydrodynamic model to explore the effect of electron and ion heating on nanoflare-heated loops. In particular, we will look at how the hot emission is affected by heating preferentially one species or the other as well as how this hot emission can vary with heating frequency, loop length, and event amplitude power-law index. We will make comparisons to results from single-fluid models in an effort to diagnose how the assumption of electron-ion equilibrium can affect conclusions about this hot emission, the so-called "smoking gun" of nanoflare heating.

## 2. METHODOLOGY

### 2.1. *Numerical Model*

1D hydrodynamic models are excellent tools for computing field-aligned quantities in coronal loops. However, because of the small grid sizes needed to resolve the transition region and consequently small timesteps needed to resolve thermal conduction, the use of such models in large parameter sweeps is made impractical by long runtimes (Bradshaw & Cargill 2013). Thus, in our numerical study, we will use a modified form of the popular 0D enthalpy-based thermal evolution of loops (EBTEL) model (Klimchuk et al. 2008; Cargill et al. 2012a,b, 2015) which computes time-dependent spatially-averaged loop quantities and has been successfully benchmarked against the 1D hydrodyhnamic HYDRAD code (Bradshaw & Cargill 2013).

We have modified the usual EBTEL equations (see Cargill et al. 2012a) to treat the evolution of the electron and ion populations separately while maintaining the assumption of quasi-neutrality, $n_e = n_i = n$. This amounts to computing spatial averages of the two-fluid hydrodynamic equations over both the transition region and corona. We will reserve a full discussion of this modified EBTEL model for a future paper. The relevant equations can be found in Appendix A.

### 2.2. *Parameter Space*

Talk about heating functions; varying heating frequency; energy budget; MC runs

We define our heating function in terms of a series of discrete heating events plus a static background heating rate to ensure that the loop does not drop to unphysically low temperatures and densities between events. All

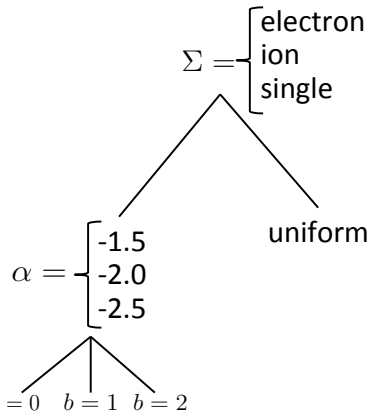


FIG. 1.— Parameter space covered for each loop half-length $L$. $\Sigma$ indicates the species that is heated, where "single" indicates a single-fluid model. $\alpha$ is the power-law index and $b$ indicates the scaling in the relationship $Q \propto T_N^b$, where $b = 0$ corresponds to the case where $T_N$ and the event energy are independent.

events are modeled as triangular pulses of fixed duration $\tau_H = 100$ s. Thus, for loop length $L$ and cross-sectional area $A$, the total energy per event is $Q_i = LAH_i\tau_H/2$, where $H_i$ is the heating rate amplitude for the $i$th event. Each run will consist of $N$ heating events, with peak amplitude $H_i$ and a steady background value of $H_b = 3.4 \times 10^{-6}$ erg cm$^{-3}$ s$^{-1}$.

Observations have suggested that loops in active region cores are maintained at an equilibrium temperature of $T_{peak} \approx 4$ MK (Warren et al. 2011, 2012). The corresponding heating rate can be estimated using coronal hydrostatics. Neglecting the radiative loss term and letting $dF_C/ds \approx \kappa_0 T_{peak}^{7/2}/L^2$, $E_{H,eq}$ can be estimated as

$$E_{H,eq} \approx \frac{\kappa_0 T_{peak}^{7/2}}{L^2}, \tag{1}$$

where $\kappa_0 \approx 10^{-6}$. $E_{H,eq}$ can be interpreted as a time-averaged volumetric heating rate. Thus, to maintain an emission measure peaked about $T_{peak}$, the individual heating rates are constrained by

$$E_{H,eq} = \frac{\tau_H}{2T}\sum_{i=1}^{N} H_i. \tag{2}$$

Note that if $H_i = H_0$ for all $i$, the uniform heating amplitude $H_0$ is just $H_0 = 2TE_{H,eq}/N\tau_H$. Thus, for $L = 40$ Mm, $A = 10^{14}$ cm$^2$, the total amount of energy injected into the loop by one heating event for a loop heated by $N = 20$ nanoflares in $T = 80000$ s is $Q = LATE_{H,eq}/N \approx 1.3 \times 10^{25}$ erg, roughly consistent with the energy budget of the Parker nanoflare model.

Determining the heating frequency in active region cores will help to place constraints on the source(s) of heat in the corona. We define the heating frequency in terms of the waiting time, $T_N$, between successive heating events. Following Cargill (2014), the range of waiting times is $250 \leq T_N \leq 5000$ s in increments of 250 s, for a total of 20 different possible heating frequencies. Additionally, $T_N$ can be written as $T_N = (T - N\tau_H)/N$, where $T = 80000$ s is the total simulation time. Note that because $T$ and $\tau_H$ are fixed, as $T_N$ increases, $N$ decreases. Correspondingly, $Q_i$, the energy injected per

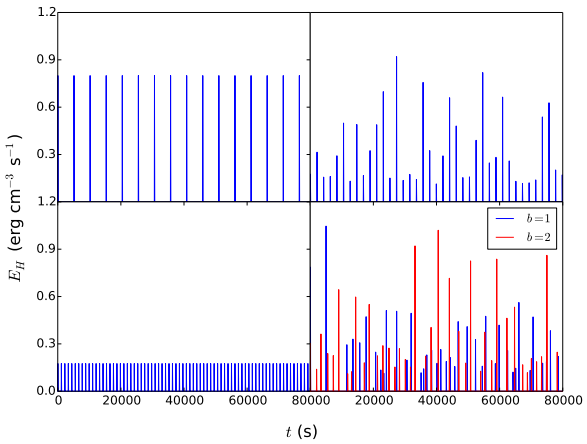


FIG. 2.— All heating functions are for $L = 40$ Mm. Starting counter-clockwise from the bottom left: uniform heating amplitudes for $T_N = 1000$ s; uniform heating amplitudes for $T_N = 5000$ s; power-law distributed heating amplitudes for $\alpha = -1.5$, $T_N = 2000$ s; power-law distributed amplitudes for $\alpha = -1.5$ where the wait times depend on the event energies and the mean wait time for both $b$ values is $\langle T_N \rangle = 2000$ s.

event, increases according to Equation 2 such that the total energy injected per run is constant, regardless of $T_N$.

We compute the peak heating rate per event in two different cases: 1) uniform heating rate such that $H_i = H_0$ for all $i$ and 2) $H_i$ chosen from a power-law distribution with index $\alpha$ where $\alpha = -1.5, -2.0, -2.5$. For the second case, it should be noted that, when $T_N$ is large, $N \sim 20$ events, meaning a single run does not accurately represent the distribution of index $\alpha$. Thus, a sufficiently large number of runs, $N_{MC}$, are computed for each $T_N$ to ensure that the total number of events is $N_{tot} = N \times N_{MC} \sim 10^4$ such that the distribution is well-represented. Figure 1 shows the parameter space we will explore. For each point in $(\Sigma, \alpha, b)$ space, the response to $\sim N_{tot}$ events for each waiting time $T_N$ will be computed.

According to the nanoflare heating model of (Parker 1988), turbulent loop footpoint motions twist and stress the field, leading to a buildup and subsequent release of energy. Following Cargill (2014), we let $Q_i \propto T_{N,i}^b$, where $Q_i, T_{N,i}$ are the total energy and waiting time following the $i$th event, respectively, and $b = 1, 2$. The reasoning for such an expression is as follows. Bursty, nanoflare heating is thought to arise from the stressing and subsequent relaxation of the coronal field. If a sufficient amount of time has elapsed since the last energy release event, the field will have had enough time to "wind up" such that the subsequent energy release is large. Conversely, if only a small amount of time has elapsed since the last event, the field will have not had time to become as stressed, resulting in a lower energy event. Thus, this scaling provides a way to incorporate a more realistic heating function into a hydrodynamic model which cannot self-consistently determine the heat input based on the evolving magnetic field. Figure 2 shows the various heating functions used for several example $T_N$ values.

## 3. RESULTS

Details about EM curves and how fits are done

### 3.1. *Electron and Ion Heating*

EM plot, derivs plot, slope plot for both species

### 3.2. *Single-fluid*

EM plot, derivs plot, slope plot

## 4. DISCUSSION

place histograms here maybe...

## 5. CONCLUSION

## APPENDIX

The modified two-fluid EBTEL equations are,

$$\frac{d}{dt}\bar{p}_e = \frac{\gamma-1}{L}[\psi_{TR} + \psi_C - (\mathcal{R}_{TR} + \mathcal{R}_C)] + k_B\bar{n}\nu_{ei}(\bar{T}_i - \bar{T}_e) + (\gamma-1)\bar{E}_{H,e}, \tag{A1}$$

$$\frac{d}{dt}\bar{p}_i = -\frac{\gamma-1}{L}(\psi_{TR} + \psi_C) + k_B\bar{n}\nu_{ei}(\bar{T}_e - \bar{T}_i) + (\gamma-1)\bar{E}_{H,i}, \tag{A2}$$

$$\frac{d}{dt}\bar{n} = \frac{c_2(\gamma-1)}{c_3\gamma L k_B \bar{T}_e}(\psi_{TR} - F_{e,0} - \mathcal{R}_{TR}), \tag{A3}$$

where

$$\psi_{TR} = \frac{1}{1+\xi}(F_{0,e} + \mathcal{R}_{TR} - \xi F_{0,i}), \tag{A4}$$

$$\psi_C = \bar{v}p_e^{(a)} - (p_e v)_0. \tag{A5}$$

Additionally, Equation A1, Equation A2, and Equation A3 are closed by the equations of state $p_e = k_B n T_e$ and $p_i = k_B n T_i$.

The volumetric heating rates, $E_{H,e}$ and $E_{H,i}$, are the primary degrees of freedom in our model. In the case of electron (ion) heating, $E_{H,i}(E_{H,e}) = 0$. $\bar{p}_e, \bar{p}_i$ and $\bar{T}_e, \bar{T}_i$ are the spatially-averaged coronal electron and ion pressures and temperatures, respectively and $\bar{n}$ is the spatially-averaged coronal number density. $\mathcal{R}_C = \bar{n}^2\Lambda(T)$ is the volumetric coronal radiative loss rate, where $\Lambda(\bar{T})$ is the radiative loss function, and $\mathcal{R}_{TR} = c_1\mathcal{R}_C$ is the radiative loss rate in

the transition region where the calculation of $c_1$ is described in Cargill et al. (2012a). Additionally, $F_{e,0}, F_{i,0}$ are the electron and ion conductive fluxes as computed at the base of the loop, respectively, and are calculated using the classical Spitzer formula with a flux limiter imposed to prevent runaway cooling at low densities. The Coulomb collision frequency, $\nu_{ei}$, is given by,

$$\nu_{ei} = \frac{16\sqrt{\pi}}{3}\frac{e^4}{m_e m_i}\left(\frac{2k_B\bar{T}_e}{m_e}\right)^{-3/2}\bar{n}\ln\Lambda, \tag{A6}$$

where $m_e, m_i$ are the electron and ion masses respectively and $\ln\Lambda$ is the Coulomb logarithm. Finally, $c_2 = \bar{T}/T_a = 0.6$, $c_3 = T_0/T_a = 0.9$, determined by static equilibrium, and $\xi = \bar{T}_e/\bar{T}_i$.

Note that in the limit that $\bar{T}_e = \bar{T}_i$ such that $\xi = 1$, Eq. Equation A3 reduces to the single-fluid density equation of Cargill et al. (2012a). Additionally, Equation A1 and Equation A2 can be added together to recover the single-fluid pressure equation. As with the original EBTEL model, the modified two-fluid version has been successfully benchmarked against the HYDRAD hydrodynamic code.

## REFERENCES


Bradshaw, S. J., & Cargill, P. J. 2006, Astronomy and Astrophysics, 458, 987

—. 2013, The Astrophysical Journal, 770, 12

Bradshaw, S. J., & Klimchuk, J. A. 2011, The Astrophysical Journal Supplement Series, 194, 26

Bradshaw, S. J., Klimchuk, J. A., & Reep, J. W. 2012, The Astrophysical Journal, 758, 53

Brosius, J. W., Daw, A. N., & Rabin, D. M. 2014, The Astrophysical Journal, 790, 112

Cargill, P. J. 1994, The Astrophysical Journal, 422, 381

—. 2014, The Astrophysical Journal, 784, 49

Cargill, P. J., Bradshaw, S. J., & Klimchuk, J. A. 2012a, The Astrophysical Journal, 752, 161

—. 2012b, The Astrophysical Journal, 758, 5

Cargill, P. J., & Klimchuk, J. A. 2004, The Astrophysical Journal, 605, 911

Cargill, P. J., Warren, H. P., & Bradshaw, S. J. 2015, Phil. Trans. R. Soc. A, 373, 20140260

Cirtain, J. W., Golub, L., Winebarger, A. R., et al. 2013, Nature, 493, 501

De Pontieu, B., Title, A. M., Lemen, J. R., et al. 2014, Solar Physics, 289, 2733

Klimchuk, J. A. 2006, Solar Physics, 234, 41

Klimchuk, J. A., Patsourakos, S., & Cargill, P. J. 2008, The Astrophysical Journal, 682, 1351

Kobayashi, K., Cirtain, J., Golub, L., et al. 2011, in Society of Photo-Optical Instrumentation Engineers (SPIE) Conference Series, Vol. 8147, 81471M

Parker, E. N. 1988, The Astrophysical Journal, 330, 474

Reale, F., & Orlando, S. 2008, The Astrophysical Journal, 684, 715

Reale, F., Testa, P., Klimchuk, J. A., & Parenti, S. 2009, The Astrophysical Journal, 698, 756

Reep, J. W., Bradshaw, S. J., & Klimchuk, J. A. 2013, The Astrophysical Journal, 764, 193

Schmelz, J. T., Saar, S. H., DeLuca, E. E., et al. 2009, The Astrophysical Journal Letters, 693, L131

Testa, P., De Pontieu, B., Martnez-Sykora, J., et al. 2013, The Astrophysical Journal Letters, 770, L1

Testa, P., De Pontieu, B., Allred, J., et al. 2014, Science, 346, 1255724

Warren, H. P., Brooks, D. H., & Winebarger, A. R. 2011, The Astrophysical Journal, 734, 90

Warren, H. P., Winebarger, A. R., & Brooks, D. H. 2012, The Astrophysical Journal, 759, 141

Winebarger, A. R. 2014, AGU Fall Meeting Abstracts, 52, 03

Winebarger, A. R., Warren, H. P., Schmelz, J. T., et al. 2012, The Astrophysical Journal Letters, 746, L17